IJCRT.ORG ISSN : 2320-2882

INTERNATIONAL JOURNAL OF CREATIVE RESEARCH THOUGHTS (IJCRT)

An International Open Access, Peer-reviewed, Refereed Journal

Numerical Investigation Of Soret-Dufour Effect And Hall Current On Casson Flow Through Porous Medium

[1]A.K. Shukla, [2]Aneesh Jayswal, [3]Mohammad Suleman Quraishi

[1]*Department of Mathematics RSKD PG College, U.P., India.*

[2]*Department of Mathematics RSKD PG College, U.P., India.*

[3]*Department of Applied Sciences, Jahangirabad Institute of Technology, U.P., India*

Abstract: Non-Newtonian fluid such as Casson fluid decodes a non-linear relationship among shear stress & shear rate. Non-Newtonian solutions are being used worldwide in medicinal and chemical industry. This research article is devoted to analyze the study of Soret-Dufour effect and Hall current on unsteady MHD Casson fluid flow model with viscous dissipation, radiation absorption past a vertical plate embedded in porous medium in the presence of radiation with heat generation/absorption. Governing equations of flow model have been non-dimensionalized for this research work, and have been solved numerically using the Crank-Nicolson implicit finite difference method. The effects of non-dimensional parameters on velocity profiles Concentration and temperature are studied with the help of graphs and tables. Furthermore, parameters like skin friction, Nusselt number and Sherwood number at dependency of various parameters are inspected through tables.

Keywords: Casson Fluid, Viscous dissipation, Magnetohydrodynamics, Order of chemical reaction, Soret and Dufour effects.

I. INTRODUCTION

Non-Newtonian fluid decodes a non-linear relationship among shear stress & shear rate. Non-Newtonian solutions are being used worldwide in medicinal and chemical industry as well such as oils, deodorizers, chemicals, syrups, Thick drinks, cleaners, processing of numerous colors etc. Several polymer liquids & salt explanations remain non-Newtonian fluids such in place of ketchup, custard, tooth-paste, flour, paint, blood, & shampoo. Newtonian fluid demonstrates a longitudinal association between shear and shear tension. Newtonian fluids cannot be represented in distinct manufacturing & additional technical requests including blood, shampoo, soap, some oils, jelly, paints etc. Several scholars, developers and scientists have investigated various applications. However, the study of non-Newtonian fluids is very complicated than Newtonian fluids. Navier–Stokes' equations cannot be evaluate directly to non-Newtonian fluid properties. Non-Newtonian fluid behavior is also used to characterize as Casson fluid model which has great importance in polymer processing industries and biomechanics. From many decades, a large number of studies of applications of Non-Newtonian fluid flow filed in the presence of different effects due to this many mathematicians have taken their great attention. Casson fluid is one of type of non-Newtonian fluid that reveals elasticity in nature, some examples of Casson fluid are honey, jelly, tomato sauce etc.. Human blood can also be treated as Casson fluid. Liaquat Ali Lund et al.[1] is investigated the magnetohydrodynamic (MHD) flow of Casson nanofluid with thermal radiation over an unsteady shrinking surface. Shahanaz Parvin et al.[2] are discussed effects of the mixed convection parameter, concentration buoyancy ratio parameter, Soret–Dufour parameters, and shrinking parameter in MHD Casson fluid flow past shrinking sheet. Lahmar et al.[3] studied heat transfer of squeezing unsteady nanofluid flow under the effects of an inclined magnetic field and variable thermal conductivity. Mohamed R.Eid et al. [4] investigated numerically for Carreau nanofluid flow over a convectively heated nonlinear stretching surface with chemically reactive species. Hammad Alotaibi et al.[5] introduced the effect of heat absorption (generation) and suction (injection) on magnetohydrodynamic (MHD) boundary-layer flow of Casson nanofluid (CNF) via a non-linear stretching surface with the viscous dissipation in two dimensions. Asogwa and Ibe [6] investigated numerical approach of MHD Casson fluid flow over a permeable stretching sheet with heat and mass transfer taking into cognizance the various parameters present. Renu et al.[7] assessed the effect of the inclined outer velocity on heat and flow transportation in boundary layer Casson fluid over a stretching sheet. Ramudu et al. [8]

highlighted the impact of magnetohydrodynamic Casson fluid flow across a convective surface with cross diffusion, chemical reaction, non-linear radiative heat. Recently Mahabaleshwar et al.[9] discussed the important roles of SWCNTs and MWCNTs under the effect of magnetohydrodynamics nanofluids flow past over the stretching/shrinking sheet under the repercussions of thermal radiation and Newtonian heating. Ram Prakash Sharma et al. [10] reports MHD Non-Newtonian Fluid Flow past a Stretching Sheet under the Influence of Non-linear Radiation and Viscous Dissipation. Naveed Akbar et al.[11] investigated Numerical Solution of Casson Fluid Flow under Viscous Dissipation and Radiation Phenomenon. Elham Alali et al. [12] studied MHD dissipative Casson nanofluid liquid film flow due to an unsteady stretching sheet with radiation influence and slip velocity phenomenon. T. M. Ajayi et al. [13] have studied Viscous Dissipation Effects on the Motion of Casson Fluid over an Upper Horizontal Thermally Stratified Melting Surface of a Paraboloid of Revolution: Boundary Layer Analysis. N. Pandya and A. K. Shukla [14] have analyzed Effects of Thermophoresis, Dufour, Hall and Radiation on an Unsteady MHD flow past an Inclined Plate with Viscous Dissipation.
In this investigation our aim is to bring to light the effect of unsteady MHD Casson fluid flow through a vertical porous plate with Soret-Dufour, Hall current, radiation absorption, heat source/sink and higher-order chemical reaction. The influence of various physical parameters on velocity, temperature and concentration profiles is discussed with the help of tables and graphs. On the other hand important physical quantities like shearing stress, Nusselt number and Sherwood number are discussed through tables.

II. MATHEMATICAL MODELING

The unsteady MHD Casson flow of a viscous incompressible electrically conducting fluid past an impulsively started infinite inclined porous plate with variable temperature and mass dispersal in the presence of radiation, radiation absorption and Hall current with viscous dissipation have been considered. The plate is vertical and is embedded in porous medium. The x- axis is taken along the plate and y-axis is taken normal to it. Initially, it is also assumed that the radiation heat flux in x- direction is negligible as compared to that in y -direction. The plate and fluid are at the same temperature and concentration. At time t, the plate is given some impulsive motion along x-direction against gravitational field with constant velocity u_0 , the plate temperature and concentration decrease exponentially with time. The transversely applied magnetic field and magnetic Reynolds number are very small and hence induced magnetic field is minute so it can be considered negligible, Cowling [16]. Due to infinite length in x-direction, the flow variables are functions of y and t only. Under the usual Boussinesq's approximation, governing partial differential equations for this unsteady flow field problem are given by:

2.1 Continuity equation:

$$\frac{\partial \bar{v}}{\partial \bar{y}} = 0 \quad \Rightarrow \quad \bar{v} = -v_0 (constant) \tag{1}$$

2.2 Momentum equation:

$$\frac{\partial \bar{u}}{\partial \bar{t}} + \bar{v}\frac{\partial \bar{u}}{\partial \bar{y}} = \nu\left(1+\frac{1}{\beta}\right)\frac{\partial^2 \bar{u}}{\partial \bar{y}^2} + g\beta_1(\bar{T}-\bar{T}_\infty) + g\beta_2(\bar{C}-\bar{C}_\infty) - \frac{\sigma B_0^{\,2} \sin^2\eta}{(1+m^2)}\bar{u} - \frac{\mu \bar{u}}{\rho_\infty \bar{K}} \tag{2}$$

2.3 Energy equation:

$$\rho_\infty C_p\left(\frac{\partial \bar{T}}{\partial \bar{t}} + \bar{v}\frac{\partial \bar{T}}{\partial \bar{y}}\right) = k\frac{\partial^2 \bar{T}}{\partial \bar{y}^2} - \frac{\partial q_r}{\partial \bar{y}} + \frac{\rho D_m K_T}{c_s}\frac{\partial^2 \bar{C}}{\partial \bar{y}^2} + \mu\left(\frac{\partial \bar{u}}{\partial \bar{y}}\right)^2 - \bar{Q}_0\left(\bar{T}-\bar{T}_\infty\right) + Q_1\left(\bar{C}-\bar{C}_\infty\right) \tag{3}$$

$$\frac{\partial \bar{C}}{\partial \bar{t}} + \bar{v}\frac{\partial \bar{C}}{\partial \bar{y}} = D\frac{\partial^2 \bar{C}}{\partial \bar{y}^2} + \frac{D_m K_T}{T_m}\frac{\partial^2 \bar{T}}{\partial \bar{y}^2} - k_r\left(\bar{C}-\bar{C}_\infty\right) \tag{4}$$

Where the term $k_r(\bar{C}-\bar{C}_\infty)$ in mass equation for first order chemical reaction, k_r is chemical reaction constant, $\bar{C}$ concentration $\bar{T}$ temperature $\bar{T}_\infty$ temperature of free stream, $\bar{C}_\infty$ concentration of free stream, β is Casson parameter, β_2 is

coefficient of volume expansion for mass transfer , β_1 is volumetric coefficient of thermal expansion, T_m mean fluid temperature, q_r radiative heat along y ∗ -axis, $\overline{Q}_0$ coefficient of heat source/sink $\overline{Q}_1$ radiation absorption parameter, ν is kinematic viscosity, $\overline{K}$ is coefficient of permeability of porous medium, D_m is molecular diffusivity, k is thermal conductivity of fluid, C_p denotes specific heat at constant pressure, μ is for viscosity, ρ fluid density, σ electrical conductivity, g is acceleration due to gravity, K_T denotes thermal diffusion ratio and m is Hall current parameter

In Equation 4; $k_r\left(\overline{C}-\overline{C}_\infty\right)$ has been taken as first order chemical reaction.

The boundary conditions for this model are assumed as:

$$\left.\begin{array}{llll} \bar{t}\le 0; & \bar{u}=0, \quad v_0=-v_0 \quad \overline{T}=\overline{T}_\infty, \quad \overline{C}=\overline{C}_\infty & & \forall\,\bar{y} \\ \bar{t}>0; & \bar{u}=u_0, \quad \overline{T}=\overline{T}_\infty+(\overline{T}_w-\overline{T}_\infty)e^{-At}, \quad \overline{C}=\overline{C}_\infty+(\overline{C}_w-\overline{C}_\infty)e^{-At} & & at\ \bar{y}=0 \\ & \bar{u}\to 0, \quad \overline{T}\to\overline{T}_\infty, \quad \overline{C}\to\overline{C}_\infty & as & \bar{y}\to\infty \end{array}\right\} \tag{5}$$

Where $A=\dfrac{v_0^{\,2}}{\nu}$

Roseland explained the term radiative heat flux approximately as

$$q_r=-\frac{4\sigma_{st}}{3a_m}\frac{\partial\overline{T}^{\,4}}{\partial\,\bar{y}^4} \tag{6}$$

Here Stefan Boltzmann constant and absorption coefficient are σ_{st} and a_m respectively.

In this case temperature differences are very-very small within flow, such that $\overline{T}^{\,4}$ can be expressed linearly with temperature. It is realized by expanding in a Taylor series about T_∞' and neglecting higher order terms, so

$$\overline{T}^{\,4}\sim=4\overline{T}_\infty^{\,3}\overline{T}-3\overline{T}_\infty^{\,4} \tag{7}$$

With the help of equations (6) and (7), we write the equation (3) in this way

$$\left.\begin{array}{l} \rho_\infty C_p\left(\dfrac{\partial\overline{T}}{\partial\bar{t}}+\bar{v}\dfrac{\partial\overline{T}}{\partial\,\bar{y}}\right)=k\dfrac{\partial^2\overline{T}}{\partial\,\bar{y}^2}+\dfrac{16\overline{T}_\infty^{\,3}\sigma_{st}}{3a_m}\dfrac{\partial^2\,\overline{T}}{\partial\,\bar{y}^2}+\dfrac{\rho D_m K_T}{c_s}\dfrac{\partial^2\overline{C}}{\partial\,\bar{y}^2} \\ +\mu\left(\dfrac{\partial\bar{u}}{\partial\,\bar{y}}\right)^2-\overline{Q}_0\left(\overline{T}-\overline{T}_\infty\right)+Q_1\left(\overline{C}-\overline{C}_\infty\right) \end{array}\right\} \tag{8}$$

Let us introduce the following dimensionless quantities

$$\left.\begin{aligned}
&u=\frac{\bar{u}}{u_0},t=\frac{\bar{t}\nu_0^{\,2}}{\nu},y=\frac{\bar{y}\nu_0}{\nu},\theta=\frac{\bar{T}-\bar{T}_\infty}{\bar{T}_w-\bar{T}_\infty},C=\frac{\bar{C}-\bar{C}_\infty}{\bar{C}_w-\bar{C}_\infty},\\
&G_m=\frac{\nu g\beta_2(\bar{C}_w-\bar{C}_\infty)}{u_0\nu_0^{\,2}},G_r=\frac{\nu\, g\beta_1(\bar{T}_w-\bar{T}_\infty)}{u_0\nu_0^{\,2}},K=\frac{\nu_0^{\,2}}{\nu^2}\bar{K},\\
&S_c=\frac{\nu}{D},P_r=\frac{\mu C_p}{k},\ M_c=\frac{\sigma B_0^{\,2}\nu\sin^2\eta}{(1+m^2)\nu_0^{\,2}},R=\frac{4\sigma\bar{T}_\infty^{\,3}}{k_m k},\\
&Q=\frac{Q_0\nu}{\rho c_p\nu_0^{\,2}},D_u=\frac{D_m K_T(\bar{C}_w-\bar{C}_\infty)}{c_s c_p\nu(\bar{T}_w-\bar{T}_\infty)},S_r=\frac{D_m K_T(\bar{T}_w-\bar{T}_\infty)}{T_m\nu(\bar{C}_w-\bar{C}_\infty)},\\
&Q_c=\frac{Q_1\nu(\bar{C}-\bar{C}_\infty)}{\rho c_p\nu_0^{\,2}(\bar{T}_w-\bar{T}_\infty)},Ec=\frac{\nu_0^{\,2}}{c_p(\bar{T}_w-\bar{T}_\infty)},A=\frac{\nu_0^{\,2}}{\nu},K_r=\frac{k_r\nu}{\nu_0^{\,2}}
\end{aligned}\right\} \quad (9)$$

Using substitutions of Equation 9, we get non-dimensional form of partial differential Equations 2, 8 and 4 respectively

$$\frac{\partial u}{\partial t}-\frac{\partial u}{\partial y}=\left(1+\frac{1}{\beta}\right)\frac{\partial^2 u}{\partial y^2}+G_r\theta+G_m C-\left(M_c+\frac{1}{K}\right)u \quad (10)$$

$$\frac{\partial\theta}{\partial t}-\frac{\partial\theta}{\partial y}=\frac{1}{P_r}\left(1+\frac{4R}{3}\right)\frac{\partial^2\theta}{\partial y^2}+D_u\frac{\partial^2 C}{\partial y^2}+Ec\left(\frac{\partial u}{\partial y}\right)^2-Q\theta-Q_c C \quad (11)$$

$$\frac{\partial C}{\partial t}-\frac{\partial C}{\partial y}=\frac{1}{S_c}\frac{\partial^2 C}{\partial y^2}+S_r\frac{\partial^2\theta}{\partial y^2}-K_r C \quad (12)$$

With initial and boundary conditions

$$\left.\begin{aligned}
&t\le 0; \quad u=0, \quad \theta=0, \quad C=0 \quad \forall y\\
&t>0; \quad u=1, \quad \theta=e^{-t}, \quad C=e^{-t} \quad at\ y=0\\
&u\to 0, \quad \theta\to 0, \quad C\to 0 \quad as\ y\to\infty
\end{aligned}\right\} \quad (13)$$

The degree of practical attention include the Skin friction coefficients τ , local Nusselt Nu, and local Sherwood Sh numbers are known as follows:

$$\tau=-\left(1+\frac{1}{\beta}\right)\left(\frac{\partial u}{\partial y}\right)_{y=0},\ N_u=-\left(\frac{\partial\theta}{\partial y}\right)_{y=0},\ Sh=-\left(\frac{\partial C}{\partial y}\right)_{y=0} \quad (14)$$

III. Numerical Method of Solution

Exact solution of system of partial differential Equations 10, 11 and 12 with boundary conditions given by Equation 13 are impossible. So, these equations we have solved by Crank-Nicolson implicit finite difference method. The Crank-Nicolson finite difference implicit method is a second order method in time ($o(\Delta t^2)$) and space, hence no restriction on space and time steps, that is, the method is unconditionally stable. The computation is executed for $\Delta y = 0.1$, $\Delta t = 0.001$ and procedure is repeated till $y = 4$. Equations 10, 11 and 12 are expressed as

$$\frac{u_{i,j+1}-u_{i,j}}{\Delta t}-\frac{u_{i+1,j}-u_{i,j}}{\Delta y}=\left(1+\frac{1}{\beta}\right)\frac{u_{i-1,j}-2u_{i,j}+u_{i+1,j}+u_{i-1,j+1}-2u_{i,j+1}+u_{i+1,j+1}}{2(\Delta y)^2}$$
$$+G_r\left(\frac{\theta_{i,j+1}+\theta_{i,j}}{2}\right)+G_m\left(\frac{C_{i,j+1}+C_{i,j}}{2}\right)-\left(M_c+\frac{1}{K}\right)\left(\frac{u_{i,j+1}+u_{i,j}}{2}\right) \quad (15)$$

$$\frac{\theta_{i,j+1}-\theta_{i,j}}{\Delta t}-\frac{\theta_{i+1,j}-\theta_{i,j}}{\Delta y}=\frac{1}{P_r}\left(1+\frac{4R}{3}\right)\left(\frac{\theta_{i-1,j}-2\theta_{i,j}+\theta_{i+1,j}+\theta_{i-1,j+1}-2\theta_{i,j+1}+\theta_{i+1,j+1}}{2(\Delta y)^2}\right)$$
$$+D_u\left(\frac{C_{i-1,j}-2C_{i,j}+C_{i+1,j}+C_{i-1,j+1}-2C_{i,j+1}+C_{i+1,j+1}}{2(\Delta y)^2}\right)+E_c\left(\frac{u_{i+1,j}-u_{i,j}}{\Delta y}\right)^2-Q\left(\frac{\theta_{i,j+1}+\theta_{i,j}}{2}\right) \quad (16)$$
$$-Q_c\left(\frac{C_{i,j+1}+C_{i,j}}{2}\right)$$

$$\frac{C_{i,j+1}-C_{i,j}}{\Delta t}-\frac{C_{i+1,j}-C_{i,j}}{\Delta y}=\frac{1}{S_C}\left(\frac{C_{i-1,j}-2C_{i,j}+C_{i+1,j}+C_{i-1,j+1}-2C_{i,j+1}+C_{i+1,j+1}}{2(\Delta y)^2}\right)$$
$$+S_r\left(\frac{\theta_{i-1,j}-2\theta_{i,j}+\theta_{i+1,j}+\theta_{i-1,j+1}-2\theta_{i,j+1}+\theta_{i+1,j+1}}{2(\Delta y)^2}\right)+K_r\left(\frac{C_{i,j+1}+C_{i,j}}{2}\right) \quad (17)$$

Initial and boundary conditions are also rewritten as:

$$u_{i,0}=0,\quad \theta_{i,0}=0,\quad C_{i,0}=0 \qquad \forall i$$
$$u_{0,j}=1,\quad \theta_{0,j}=e^{-j\Delta t},\quad C_{0,j}=e^{-j\Delta t} \qquad \forall j \quad (18)$$
$$u_{l,j}\to 0,\quad \theta_{l,j}\to 0,\quad C_{l,j}\to 0$$

Where index i represents to y and j represents to time t, $\Delta t = tj+1-tj$ and $\Delta y = yi+1-yi$. Getting the values of u, θ and C at time t, we may compute the values at time $t+\Delta t$ as following method: we substitute i = 1, 2, ..., l−1 , where n correspond to ∞ ,equations 15 to 17 give tridiagonal system of equations with boundary conditions in equation 18, are solved employing Thomas algorithm as discussed in Carnahan et al.[15], we find values of θ and C for all values of y at $t + \Delta t$. Equation 15 is solved by same to substitute these values of θ and C, we get solution for u till desired time t.

IV. ANALYSIS OF RESULTS

The present work analyzes the boundary layer unsteady MHD Casson flow past a porous vertical plate with the Soret-Dufour effect with Hall current. The influence of the first order chemical reaction has been incorporated in the mass equation. In order to see a physical view of work, numerical results of velocity profile u, temperature profile θ, concentration profile C have been discussed with the help of graphs and skin friction coefficients, Nusselt number and Sherwood number are discussed with the help of tables. The following values are used for investigation Gr = 5.5, Gm = 5 and K = 2, Mc = 0.3, β= 0.5. It is noted from figure 2 that increasing radiation parameter R, velocity u increases. This is correct observation because the increase in radiation reveals heat energy to flow. In figure 5, velocity decreases as Prandtl number Pr increases and temperature decreases in figure 11 when Pr increases. In figure 23 concentration C near to plate decreases and some distance from plate concentration increases as Prandtl number increases. Figure 16 depicts the importance of radiation on temperature distribution. It is analyzed that an increase in R, temperature θ increases and it is notable that an increase in R, concentration C near to plate decrease after that increases in figure 20. Figure 19 depicts the variation of Schmidt number Sc as concentration decreases rapidly with increase Sc while it is noteworthy that on increasing Schmidt numbers Sc velocity profile in figure 8 decreases near to plate. In figure 7, 15 and 26, it is seen that velocity increases and temperature increases as increase Dufour number Du, whereas concentration decreases as Du increases. In figure 9, 18 and 28, it is seen that velocity temperature and concentration increases as increase in Soret number Sr. Figures 6 and 24 depict the behavior of chemical reaction parameter Kr on velocity and concentration respectively. It is seen that velocity decreases, concentration decreases rapidly as Kr increase. It is observe that on increasing Casson parameter β, velocity profile decreases rapidly in Figure 10. The negative value of $Q < 0$ means heat absorption and the positive value of $Q > 0$ means heat transfer. In figure 3, velocity profile decreases on increasing heat source/sink parameter Q and also reducing momentum boundary layer. Figure 13 analyzed the impact of heat source/sink parameter Q in the temperature profile. It can be seen that the temperature profile decreases rapidly and the thermal boundary layer reduces for an increase of heat source parameter but it increases with the heat sink parameter. Figure 22, depicts that concentration profile increases near to plate from middle of boundary layer it decreases as well as species boundary layer reduces on an increase of heat source/sink parameter. The influence of Radiation absorption parameter Q_c on the velocity, temperature and concentration profiles in figure 4, 12 and figure 21 have been shown. We observe that when an increase Q_c results in the concentration profile also decreases while velocity and temperature increases. Figure 1, 17 and 27 reveals that velocity, temperature and concentration increase on increase of time. Figure 14 and 25 described that increment in Ec results in temperature increases and concentration decreases.

It is observed from **Table 1** that Change in Schmidt number Sc effects as skin friction coefficient and Sherwood number increases while Nusselt number decreases. Pr effects as skin friction coefficient and Nusselt number decreases while Sherwood number increases. Skin friction coefficient and Sherwood number increases whereas Nusselt number increases with Dufour number Du increases and radiation parameter R increase. Increase in Soret number Sr, Skin friction and Sherwood number increase while Nusselt number Nu decreases. On increasing Casson fluid parameter β results in skin friction and Nusselt number decreases while Sherwood number increases. It is also noted that increment in Q heat source/sink the skin friction coefficient and Nusselt number increases while Sherwood number decreases. Skin friction coefficient and Sherwood number increases whereas Nusselt number decreases when Qc heat absorption parameter increase. Increase in Eckert number affects the increment in Skin friction and Sherwood number while Nusselt number decreases.

V. CONCLUSION

Effect of viscous dissipation, first order chemical reaction, change in Soret-Dufour and Hall current effects on unsteady MHD flow past a vertical porous plate immersed in a porous medium are analyzed. This investigation the following conclusions have come:

5.1 The effect of radiation on concentration is noteworthy. It is observed that increasing values of R, concentration falls down and after some distance from the plate, it goes up slowly-slowly.

5.2 Interestingly, the change in concentration has been found first increases then decreases on increasing Prandtl number P r.

5.3 For increasing values of Kr, it is a considerable enhancement in velocity, i.e. velocity decreases slowly.

5.4 Increasing values of Dufour number, it is observed that velocity and temperature profile in the thermal boundary layer increases whereas concentration profile first decreases after then increases slowly in the boundary layer.

5.5 Schmidt number greatly influences the concentration profile in the concentration boundary layer.

5.6 On increment in Eckert number Ec velocity and temperature increases and concentration decreases.

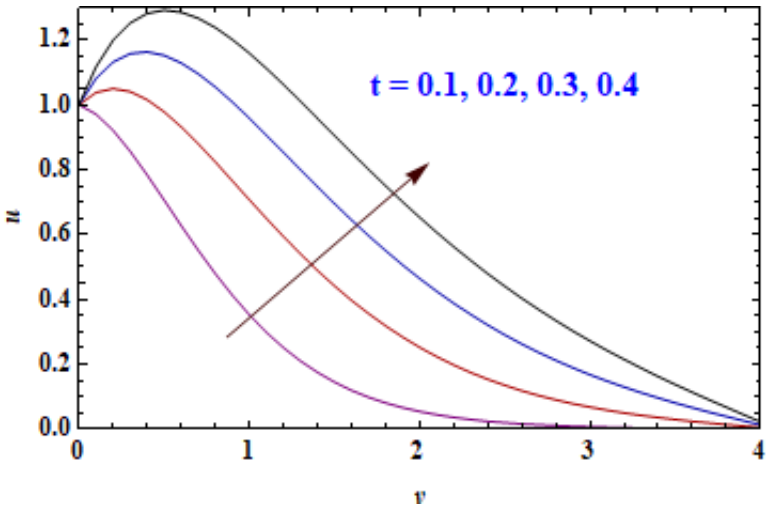

Fig. 1 Velocity Profiles for Different Values of t

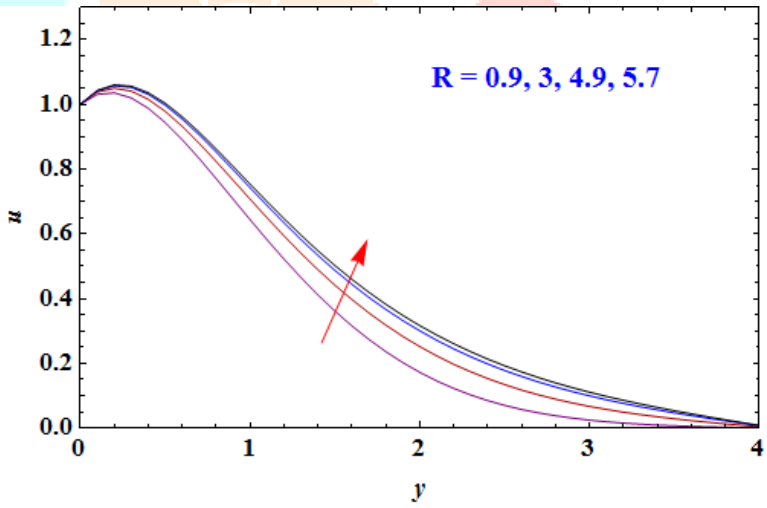

Fig. 2 Velocity Profiles for Different Values of R

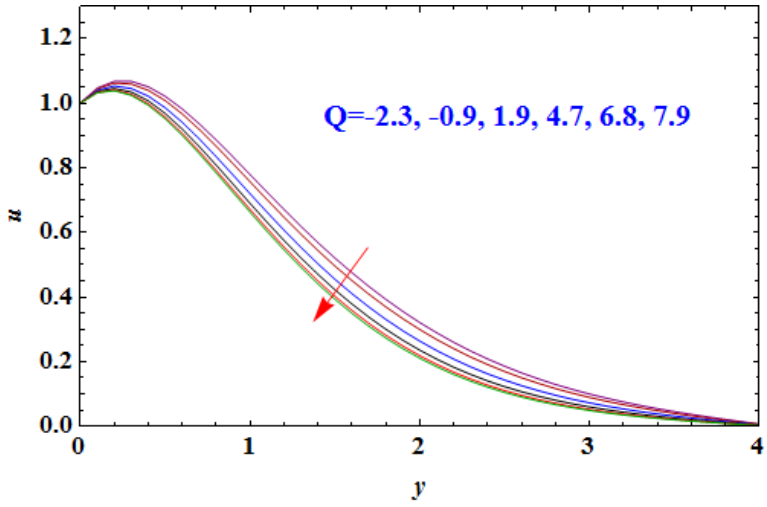

Fig. 3 Velocity Profiles for Different Values of Q

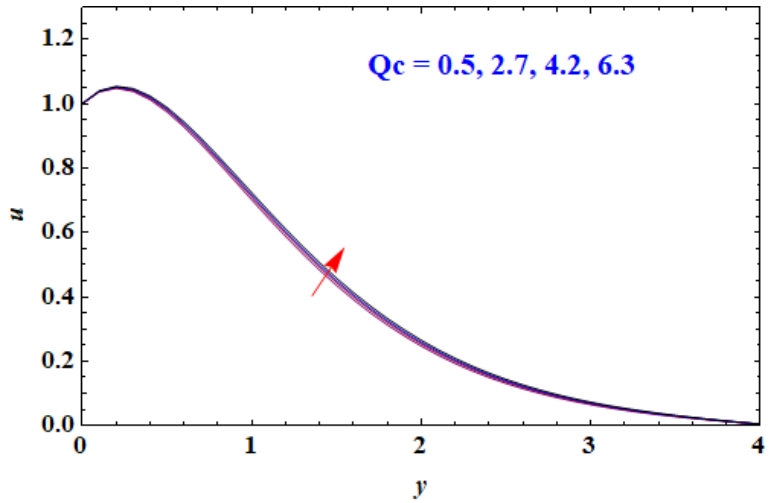

Fig. 4 Velocity Profiles for Different Values of Qc

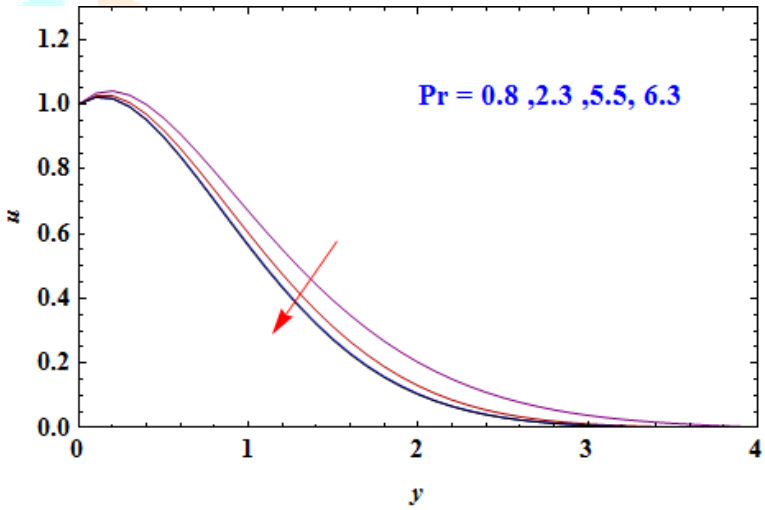

Fig. 5 Velocity Profiles for Different Values of Pr

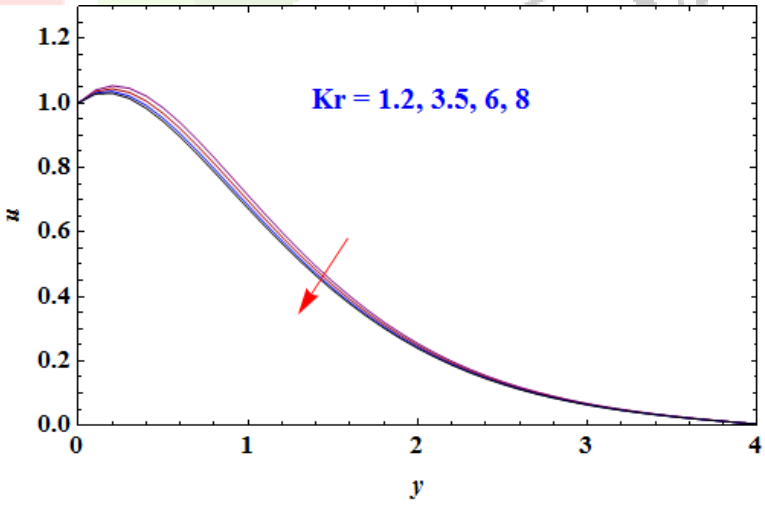

Fig. 6 Velocity Profiles for Different Values of Kr

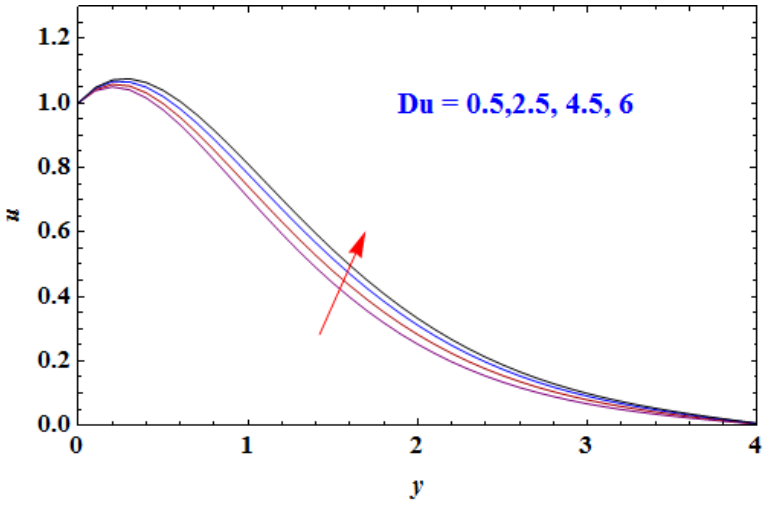

Fig. 7 Velocity Profiles for Different Values of Du

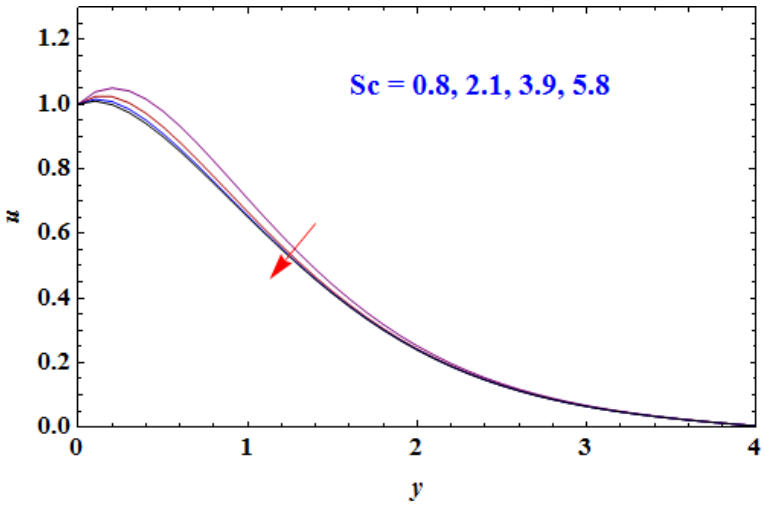

Fig. 8 Velocity Profiles for Different Values of Sc

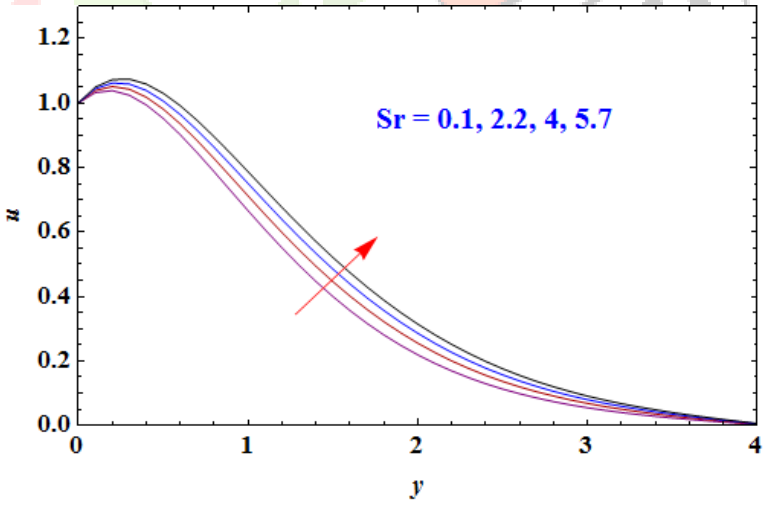

Fig. 9 Velocity Profiles for Different Values of Sr

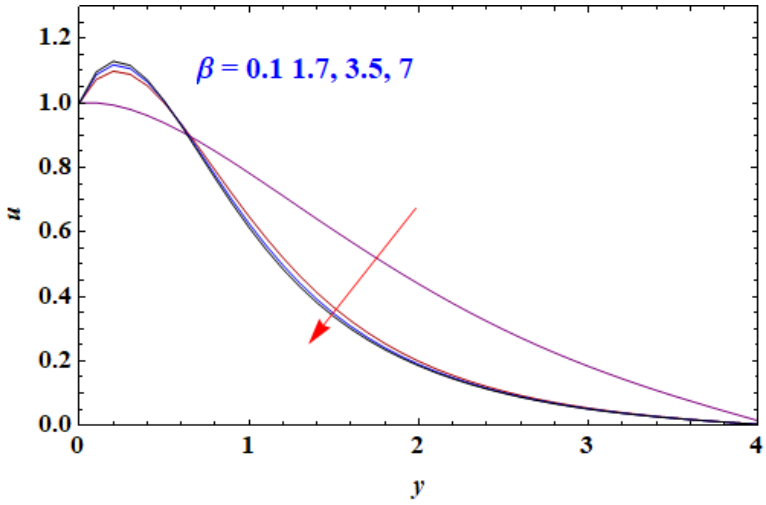

Fig. 10 Temperature Profiles for Different Values of β

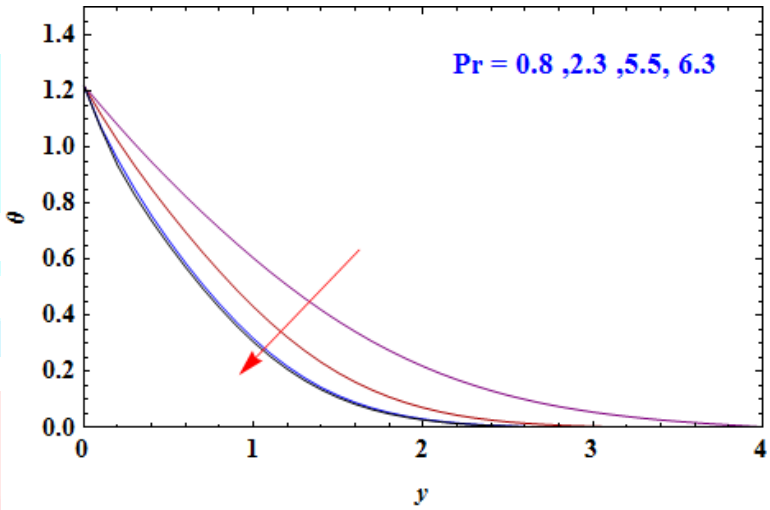

Fig. 11 Temperature Profiles for Different Values of Pr

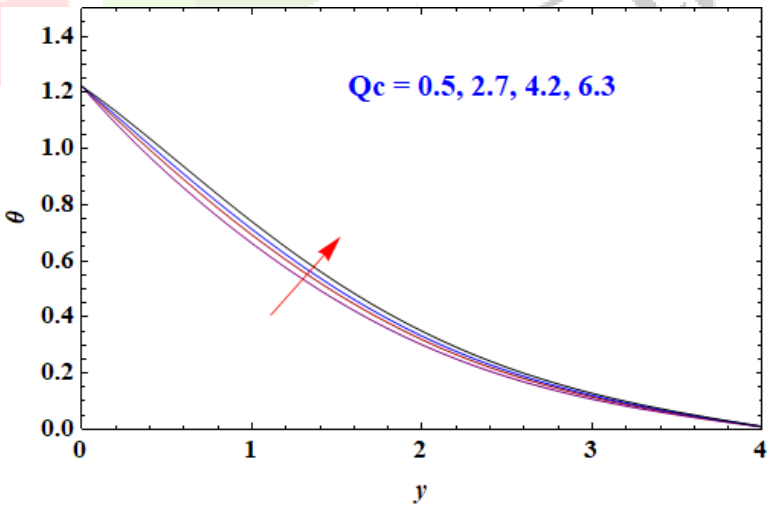

Fig. 11 Temperature Profiles for Different Values of Qc

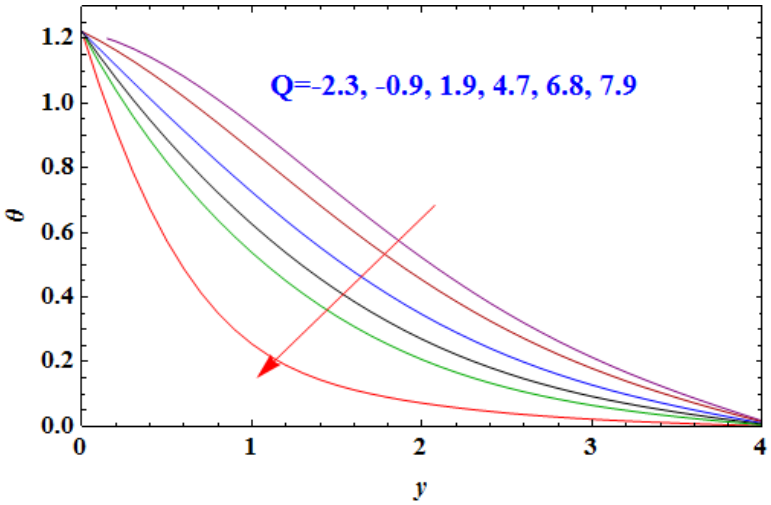

Fig. 12 Temperature Profiles for Different Values of Q

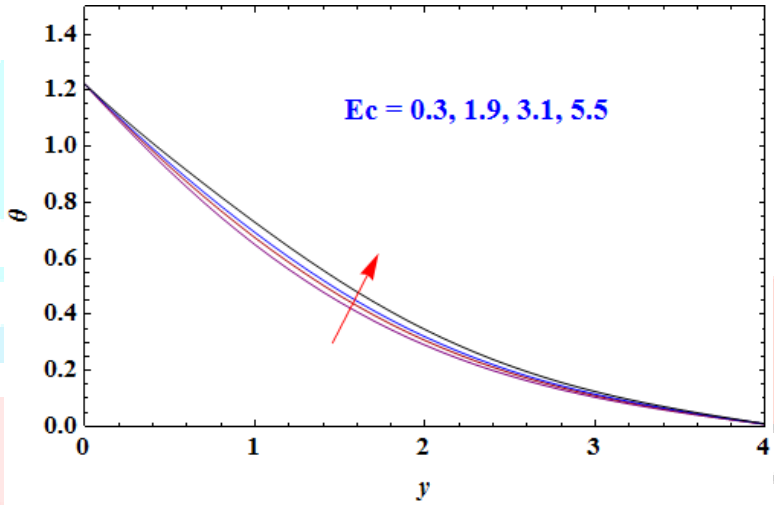

Fig. 13 Temperature Profiles for Different Values of Ec

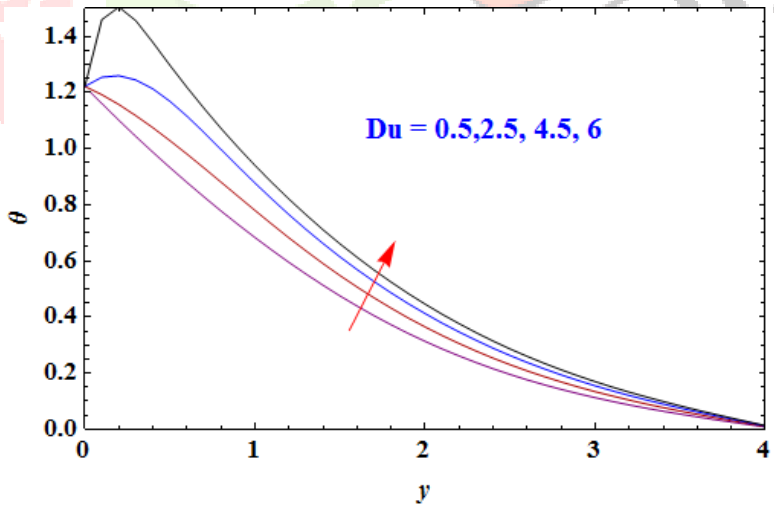

Fig. 14 Temperature Profiles for Different Values of Du

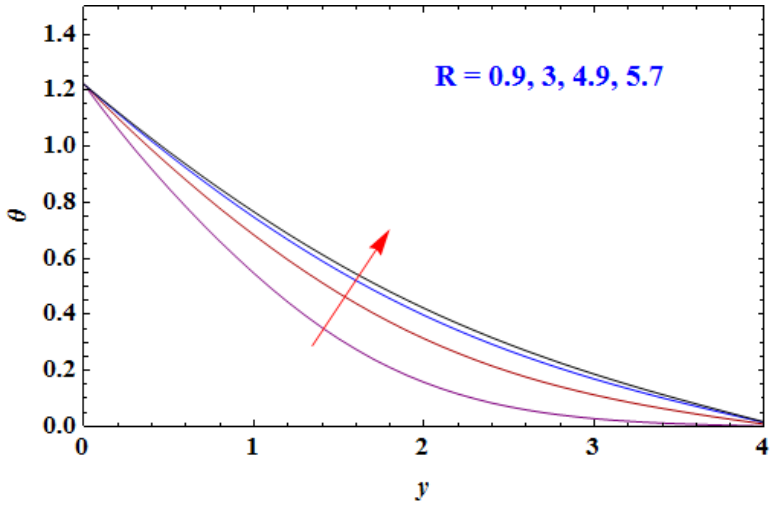

Fig. 15 Temperature Profiles for Different Values of R

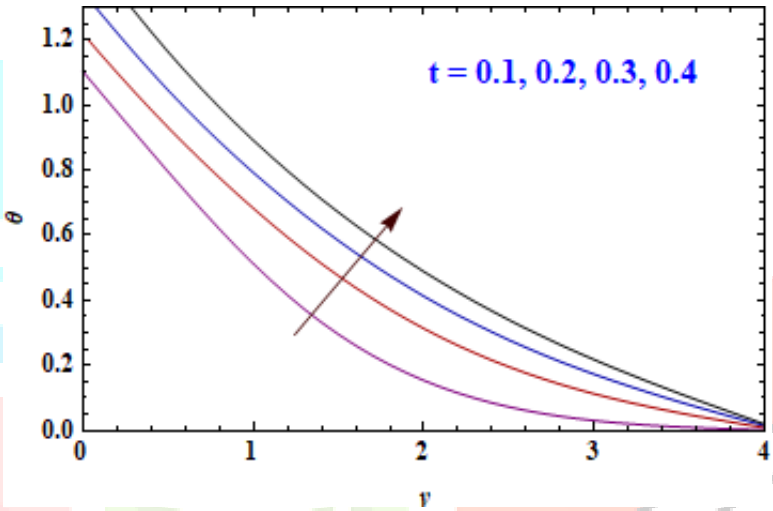

Fig. 16 Temperature Profiles for Different Values of t

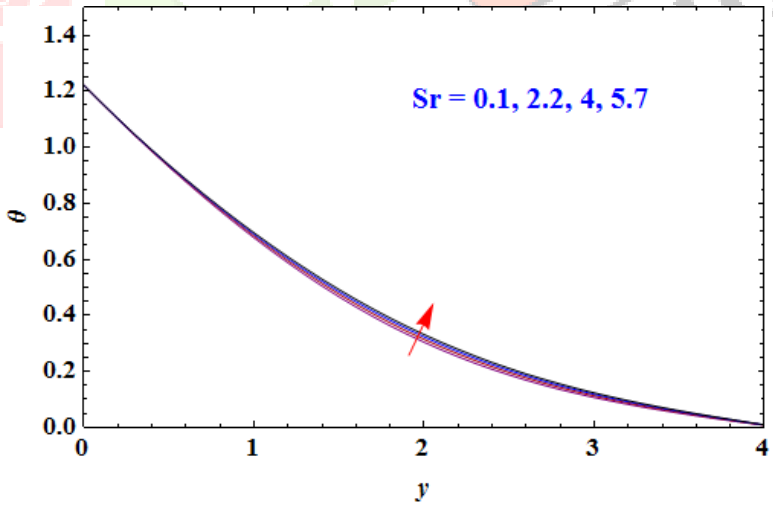

Fig. 17 Temperature Profiles for Different Values of Sr

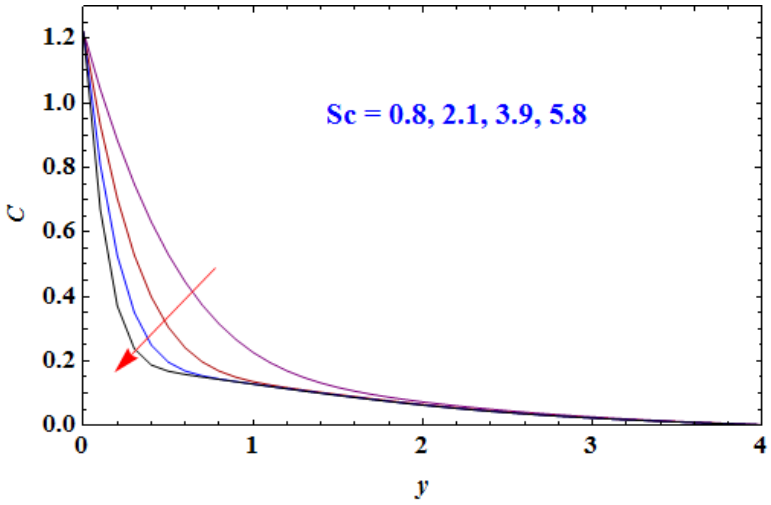

Fig. 18 Concentration Profiles for Different Values of Sc

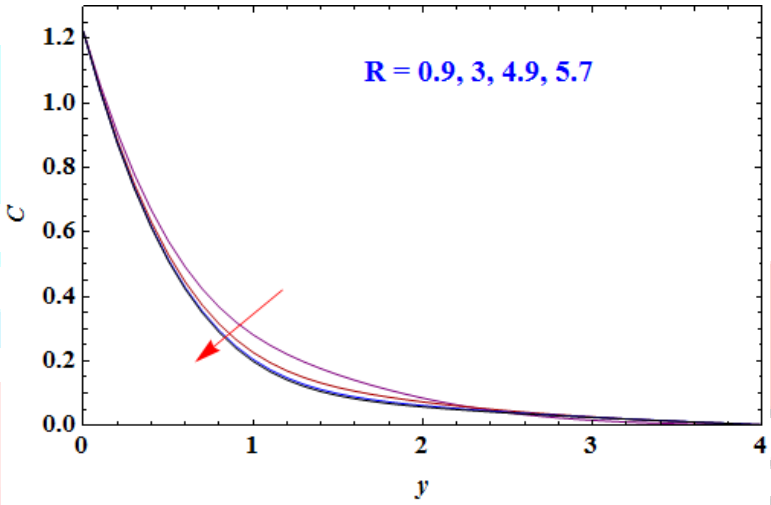

Fig. 19 Concentration Profiles for Different Values of R

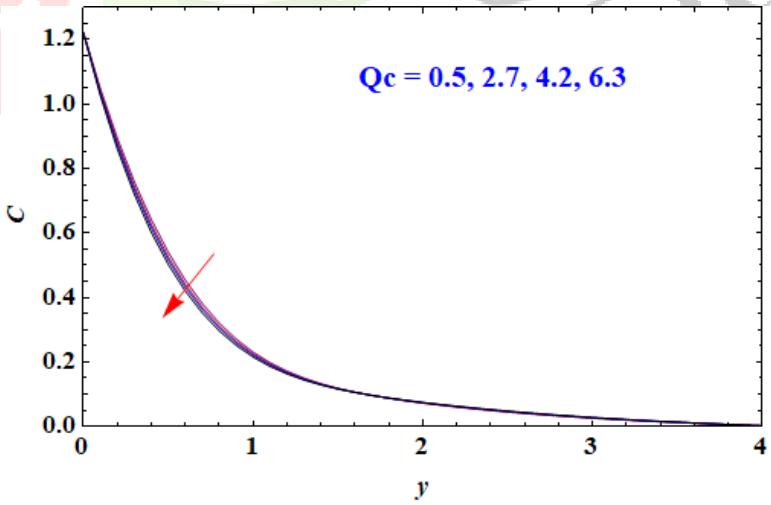

Fig. 20 Concentration Profiles for Different Values of Qc

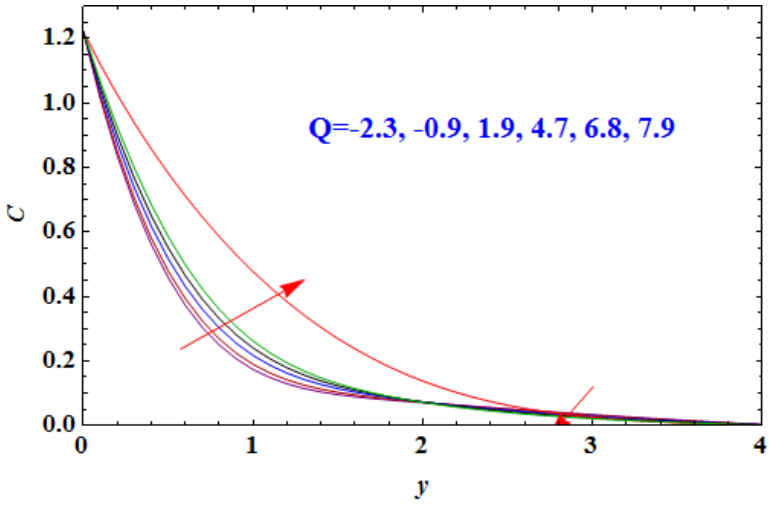

Fig. 21 Concentration Profiles for Different Values of Q

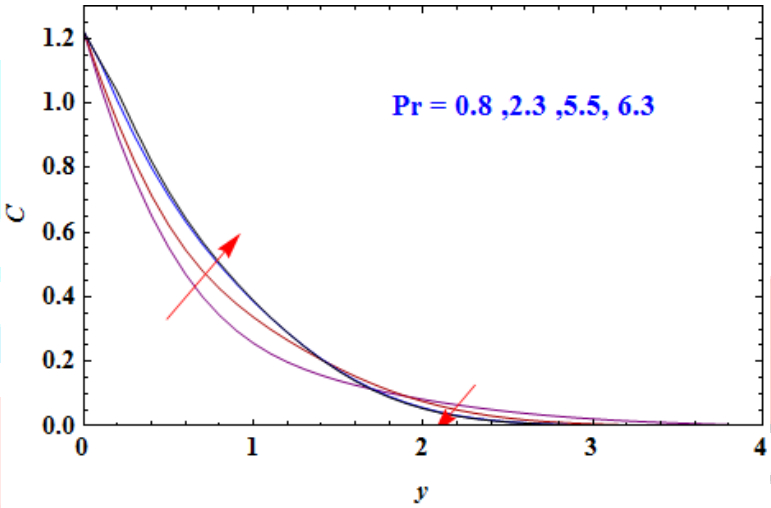

Fig. 22 Concentration Profiles for Different Values of Pr

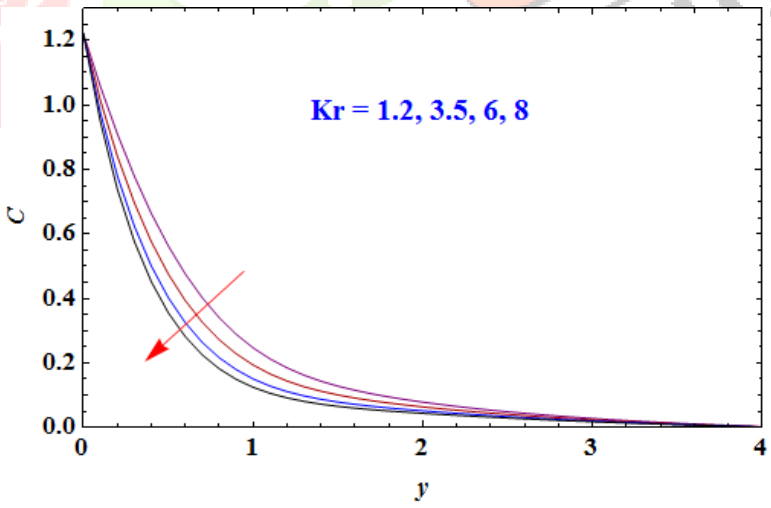

Fig. 23 Concentration Profiles for Different Values of Kr

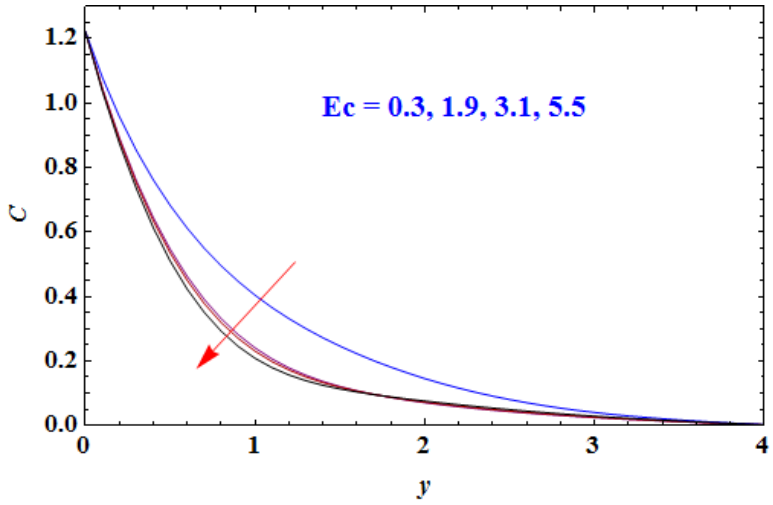

Fig. 24 Concentration Profiles for Different Values of Ec

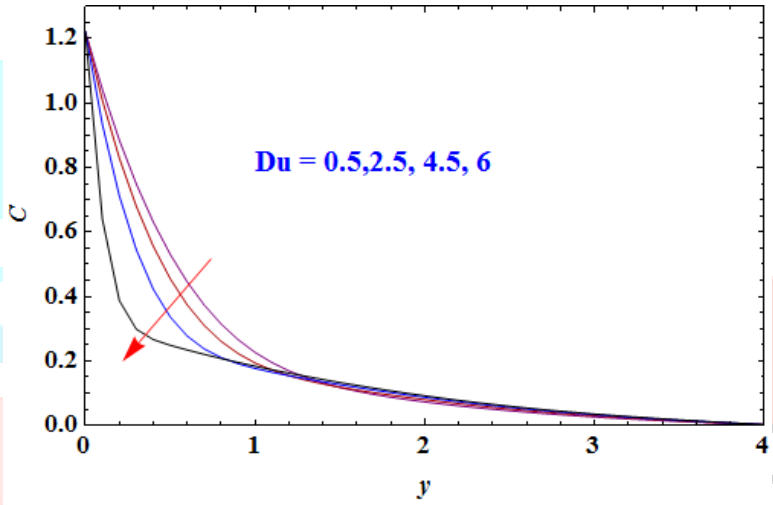

Fig. 25 Concentration Profiles for Different Values of Du

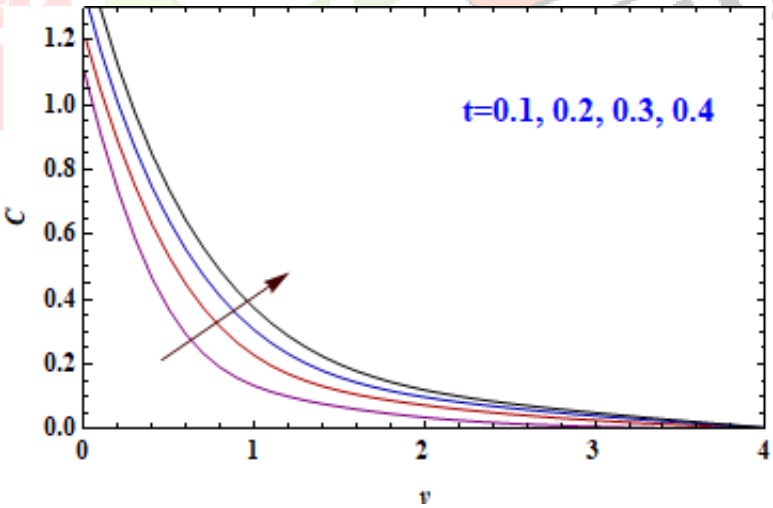

Fig. 26 Concentration Profiles for Different Values of t

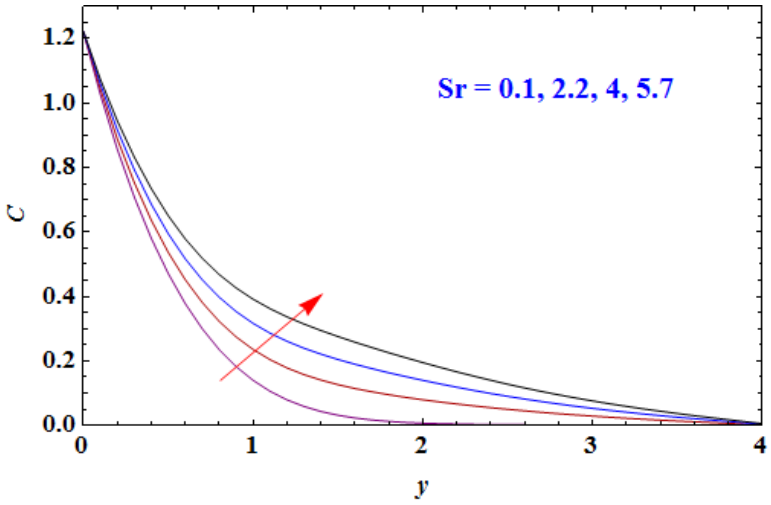

Fig. 27 Concentration Profiles for Different Values of Sr

Table 1. Skin friction coefficient τ, Nusselt number Nu and Sherwood number Sh for different values of parameters taking fix values of Gr = 5.5, Gm = 5, K = 2,

β	Du	Kr	Pr	Q	Q_c	S_c	R	S_r	t	Ec	Mc	τ	Nu	Sh
0.1	0.5	2	0.5	3	2	0.8	3	2	0.2	2.5	0.3	0.044668	0.634181	1.77644
1.7	0.5	2	0.5	3	2	0.8	3	2	0.2	2.5	0.3	1.15698	0.591446	1.81243
3.5	0.5	2	0.5	3	2	0.8	3	2	0.2	2.5	0.3	1.12482	0.584132	1.81871
7	0.5	2	0.5	3	2	0.8	3	2	0.2	2.5	0.3	1.10113	0.579815	1.82244
0.5	0.5	2	0.5	3	2	0.8	3	2	0.2	2.5	0.3	1.13797	0.609966	1.79675
0.5	2.5	2	0.5	3	2	0.8	3	2	0.2	2.5	0.3	-1.14836	0.550275	1.18127
0.5	4.5	2	0.5	3	2	0.8	3	2	0.2	2.5	0.3	1.37702	-0.325679	2.87812
0.5	6	2	0.5	3	2	0.8	3	2	0.2	2.5	0.3	1.44202	-2.37809	5.81263
0.5	0.5	1.2	0.5	3	2	0.8	3	2	0.2	2.5	0.3	1.19205	0.613364	1.63953
0.5	0.5	3.5	0.5	3	2	0.8	3	2	0.2	2.5	0.3	1.04603	0.603874	2.06654
0.5	0.5	6	0.5	3	2	0.8	3	2	0.2	2.5	0.3	0.915893	0.594445	2.45601
0.5	0.5	8	0.5	3	2	0.8	3	2	0.2	2.5	0.3	0.828621	0.587473	2.72441
0.5	0.5	2	0.8	3	2	0.8	3	2	0.2	2.5	0.3	1.01138	0.720099	1.73181
0.5	0.5	2	2.3	3	2	0.8	3	2	0.2	2.5	0.3	0.780428	1.02943	1.48536
0.5	0.5	2	5.5	3	2	0.8	3	2	0.2	2.5	0.3	0.661756	1.48866	0.982672
0.5	0.5	2	6.3	3	2	0.8	3	2	0.2	2.5	0.3	0.64933	1.52423	0.959504
0.5	0.5	2	0.5	-2.3	2	0.8	3	2	0.2	2.5	0.3	-1.40728	0.126178	2.08936
0.5	0.5	2	0.5	-0.9	2	0.8	3	2	0.2	2.5	0.3	-1.3246	0.271277	2.00795
0.5	0.5	2	0.5	1.9	2	0.8	3	2	0.2	2.5	0.3	-1.18499	0.522712	1.85421
0.5	0.5	2	0.5	4.7	2	0.8	3	2	0.2	2.5	0.3	-1.0725	0.734434	1.71084
0.5	0.5	2	0.5	6.8	2	0.8	3	2	0.2	2.5	0.3	-1.00192	0.873511	1.60913
0.5	0.5	2	0.5	7.9	2	0.8	3	2	0.2	2.5	0.3	-0.968839	0.940874	1.55762
0.5	0.5	2	0.5	3	0.5	0.8	3	2	0.2	2.5	0.3	1.11465	0.676082	1.74078
0.5	0.5	2	0.5	3	2.7	0.8	3	2	0.2	2.5	0.3	1.14871	0.5796	1.82255
0.5	0.5	2	0.5	3	4.2	0.8	3	2	0.2	2.5	0.3	1.1714	0.51555	1.87716
0.5	0.5	2	0.5	3	6.3	0.8	3	2	0.2	2.5	0.3	1.20248	0.42816	1.95213
0.5	0.5	2	0.5	3	2	0.8	3	2	0.2	2.5	0.3	1.13797	0.609966	1.79675
0.5	0.5	2	0.5	3	2	2.1	3	2	0.2	2.5	0.3	0.714601	0.583124	2.90226
0.5	0.5	2	0.5	3	2	3.9	3	2	0.2	2.5	0.3	0.457208	0.537363	4.14355
0.5	0.5	2	0.5	3	2	5.8	3	2	0.2	2.5	0.3	0.287508	0.478243	5.53112
0.5	0.5	2	0.5	3	2	0.8	0.9	2	0.2	2.5	0.3	0.925171	0.811559	1.66889
0.5	0.5	2	0.5	3	2	0.8	3	2	0.2	2.5	0.3	1.13797	0.609966	1.79675
0.5	0.5	2	0.5	3	2	0.8	4.9	2	0.2	2.5	0.3	1.25425	0.525434	1.83953
0.5	0.5	2	0.5	3	2	0.8	5.7	2	0.2	2.5	0.3	1.2918	0.500973	1.85113
0.5	0.5	2	0.5	3	2	0.8	3	0.1	0.2	2.5	0.3	0.964898	0.613522	1.94909
0.5	0.5	2	0.5	3	2	0.8	3	2.2	0.2	2.5	0.3	1.15631	0.609575	1.78032
0.5	0.5	2	0.5	3	2	0.8	3	4	0.2	2.5	0.3	1.32241	0.605908	1.62911
0.5	0.5	2	0.5	3	2	0.8	3	5.7	0.2	2.5	0.3	1.48101	0.602204	1.48094
0.5	0.5	2	0.5	3	2	0.8	3	2	0.1	2.5	0.3	-0.869446	0.627965	1.97885

0.5	0.5	2	0.5	3	2	0.8	3	2	0.2	2.5	0.3	1.13797	0.609966	1.79675
0.5	0.5	2	0.5	3	2	0.8	3	2	0.3	2.5	0.3	2.43473	0.636813	1.85643
0.5	0.5	2	0.5	3	2	0.8	3	2	0.4	2.5	0.3	3.51011	0.675098	2.00444
0.5	0.5	2	0.5	3	2	0.8	3	2	0.2	0.3	0.3	1.10012	0.656115	1.75968
0.5	0.5	2	0.5	3	2	0.8	3	2	0.2	1.9	0.3	1.12772	0.622365	1.78678
0.5	0.5	2	0.5	3	2	0.8	3	2	0.2	3.1	0.3	1.14818	0.597703	1.80661
0.5	0.5	2	0.5	3	2	0.8	3	2	0.2	5.5	0.3	-1.69204	-1.16759	1.72165
0.5	0.5	2	0.5	3	2	0.8	3	2	0.2	5.5	0.3	1.13797	0.609966	1.79675
0.5	0.5	2	0.5	3	2	0.8	3	2	0.2	5.5	2.9	2.3284	0.604148	1.79699
0.5	0.5	2	0.5	3	2	0.8	3	2	0.2	5.5	6.1	2.45755	0.602994	1.79757
0.5	0.5	2	0.5	3	2	0.8	3	2	0.2	5.5	8.3	2.47688	0.602805	1.79766

VI. ACKNOWLEDGMENT

We acknowledge our principal dr. V. C. Tripathi and chief proctor of science faculty dr a. K. Dwivedi and thank for encouraging to complete this research work.

REFERENCES

[1] Shafiq A., Rasool G. and Tlili I. 2020. Marangoni convective nanofluid flow over an electromagnetic actuator in the presence of first-order chemical reaction. Heat Transf. Asian Res .49: 274–288.

[2] Parvin S.; Mohamed Isa S.S.P., Arifin, N.M., Md Ali, F. 2021. The Inclined Factors of Magnetic Field and Shrinking Sheet in Casson Fluid Flow. Heat and Mass Transfer Symmetry. 13(373), https://doi.org/10.3390/ sym13030373.

[3] Lahmar Sihem, Kezzar Mohamed, Eid Mohamed R., and Sari, Mohamed Rafik 2020. Heat transfer of squeezing unsteady nanofluid flow under the effects of an inclined magnetic field and variable thermal conductivity. Physica A: Statistical Mechanics and its Applications, Elsevier. 540(C)

[4] M. R. Eid, K. Mahny, A. Dar and T. Muhammad .2020. Numerical study for Carreau nanofluid flow over aconvectively heated nonlinear stretching surface with chemically reactive species. Physica A: Statistical Mechanics and Its Applications. 540(123063).

[5] Hammad Alotaibi, Saeed Althubiti, Mohamed R. Eid, K. L. Mahny. 2021. Numerical Treatment of MHD Flow of Casson Nanofluid via Convectively Heated Non-Linear Extending Surface with Viscous Dissipation and Suction/Injection Effects. 66(1): 229-245, doi:10.32604/cmc.2020.012234.

[6] K. K. Asogwa and A. A. Ibe. 2020. A Study of MHD Casson Fluid Flow over a Permeable Stretching Sheet with Heat and Mass Transfer. Journal of Engineering Research and Reports. 16(2): 10-25.

[7] Renu Devi, Vikas Poply, Manimala. 2021. Effect of aligned magnetic field and inclined outer velocity in casson fluid flow over a stretching sheet with heat source. Journal of Thermal Engineering.7(4): 823-844.

[8] K Kumar Anantha, , Ankalagiri Ramudu Sugunamma Vangala, Dr.N. Sandeep. 2021. Impact of Soret and Dufour on MHD Casson fluid flow past a stretching surface with convective-diffusive conditions. Journal of Thermal Analysis and Calorimetry 10.1007/s10973-021-10569-w.

[9] U. S. Mahabaleshwar, K. N. Sneha, Akio Miyara, M. Hatami. 2022. Radiation effect on inclined MHD flow past a super-linear stretching/shrinking sheet including CNTs, Waves in Random and Complex Media. DOI: 10.1080/17455030.2022.2053238.

[10] Ram Prakash Sharma and Sachin Shaw. 2022. MHD Non-Newtonian Fluid Flow past a Stretching Sheet under the Influence of Non-linear Radiation and Viscous Dissipation. J. Appl. Comput. Mech.8(3): 949-961.

[11] Naveed Akbar, Sardar Muhammad Hussain and Riaz Ullah Khan. 2022. Numerical Solution of Casson Fluid Flow under Viscous Dissipation and Radiation Phenomenon. Journal of Applied Mathematics and Physics. 10: 475-490.

[12] Elham Alali Elham Alali and Ahmed M. Megahed. 2022. MHD dissipative Casson nanofluid liquid film flow due to an unsteady stretching sheet with radiation influence and slip velocity phenomenon. Nanotechnology Reviews. 11: 463–472

[13] T. M. Ajayi, A. J. Omowaye, and I. L. Animasaun. 2017. Viscous Dissipation Effects on the Motion of Casson Fluid over an Upper Horizontal Thermally Stratified Melting Surface of a Paraboloid of Revolution: Boundary Layer Analysis. Hindawi Journal of Applied Mathematics. 2017: https://doi.org/10.1155/2017/1697135.

[14] N. Pandya and A. K. Shukla. 2014. Effects of Thermophoresis, Dufour, Hall and Radiation on an Unsteady MHD flow past an Inclined Plate with Viscous Dissipation. International Journal of Mathematics and Scientific Computing. 4(2).

[15] Brice Carnahan, H.A. Luther and James O. Wilkes.1990. Applied Numerical Methods, Krieger Pub Co, Florida.

[16] T. G. Cowling. 1990. Magneto-Hydrodynamics, Inter Science Publishers, New York.